

Precise Physical Parameters, Habitability, and Orbital Stability of Sun-like SB2 Systems: HD 130669, HD 184467, HD 191854, and HD 214222

Ahmad Abushattal¹, Nikolaos Georgakarakos^{2,3}, Mashhoor A. Al-Wardat⁴,
Bilal Algnamat¹, Hassan B. Haboubi⁴, Deshinta Arrova Dewi⁵,
Enas M. Abu-Alrob⁶, and Abdallah M. Hussein⁶

¹Department of Physics, Al-Hussein Bin Talal University, PO Box 20, 71111, Ma'an, Jordan

²Division of Science, New York University Abu Dhabi, Abu Dhabi, UAE

³Center for Astrophysics and Space Science (CASS), New York University, Abu Dhabi, PO Box 129188, Abu Dhabi, UAE

⁴Department of Applied Physics and Astronomy, and Sharjah Academy for Astronomy, Space Sciences and Technology, University of Sharjah, PO Box 27272, Sharjah, UAE

⁵Faculty of Data Science and Information Technology, INTI International University, Malaysia

⁶Department of Physics, Faculty of Sciences, Al al-Bayt University, Mafraq, Jordan

December 30, 2025

Abstract

This work analyzes four Sun-like double-lined spectroscopic binary (SB2) systems by combining visual and spectroscopic observational data with Al-Wardat's atmospheric modeling method to accurately determine their fundamental parameters. For each system, we determine stellar masses, orbital parallaxes, effective temperatures, spectral types, semimajor axes, and eccentricities with high precision, resolving discrepancies between astrometric and spectroscopic measurements. Moreover, we assess the potential for stable planetary orbits in these systems. We also calculate habitable zones around these binaries based on the orbital evolution of planetary orbits. These systems may represent promising targets for future extrasolar planet searches around Sun-like stars due to their robust physical and orbital parameters that can be used to determine planetary habitability and stability.

Unified Astronomy Thesaurus concepts: Spectroscopic binary stars (1557); Habitable zone (696); Visual binary stars (1777)

1 Introduction

1.1 Importance and Prevalence of Binary Systems

The coming generations of telescopes and space missions will lead to discoveries that will answer many questions about the formation and dynamic evolution processes of binary and multiple stars. They will also prove helpful in searching for stellar and planetary companions of those stars, especially Earth-like ones. Statistically, it has become rather clear that most of the nearby stars are members of binary and multiple stellar systems, which form in the early stages of star formation (A. Duquennoy and M. Mayor 1991; D. Raghavan et al. 2010; G. Duchene and A. Kraus 2013; D. Jack et al. 2020; B. Algnamat et al. 2022; H. Alameryeen et al. 2022; S. Alnaimat et al. 2025). Multiple-star system analysis is an active field of research aimed at understanding the origin and evolution of stellar systems (E. P. Horch et al. 2009; G. Duchene and A. Kraus 2013; A. Tokovinin 2014; A. Tokovinin and E. P. Horch 2016; J. A. Docobo et al. 2017; R. A. Matson et al. 2018; A. Taani et al. 2019; A. Tokovinin et al. 2019; L. Piccotti et al. 2020). We can calculate the telescope size required to visually resolve spectroscopic binaries by estimating the angular size of the photocentric orbit (S. Ren and Y. Fu 2010; A. A. M. Abushattal 2017; A. A. Abushattal et al. 2019b).

1.2 Astrometric Missions and Data Importance

Hipparcos and Gaia, as European Space Agency (ESA) space-astrometric missions, are considered some of the most essential achievements in the space sciences over the past decades. They constitute the cornerstone and a significant source of information covering various astronomical fields. These missions give the positions, color indices, motion, distances, and other data for millions of stars (M. Perryman et al. 1997; F. van Leeuwen 2007; T. Prusti et al. 2016; Gaia Collaboration 2018a). The parallax is one of the most essential pieces of information these space missions provide. It is an important factor in the analysis of multiple and binary stars. Based on the well-known Kepler's third law, the catalogs of these missions use the parallaxes to estimate the total mass of visual binaries.

1.3 Discrepancies in Parallax and Complementary Methods

In recent years, there have been discrepancies between the parallaxes for the respective space missions Hipparcos and Gaia (see Table 1). The accuracy of these parallaxes, together with accurate measurements of the orbital elements, period, and semimajor axis, will help calculate the most accurate total masses for the binaries (J. C. Zinn et al. 2017; R. Drimmel et al. 2019; E. Vasiliev 2019; M. A. Al-Wardat et al. 2021a; M. A. Fardal et al. 2021). In recent years, hundreds of research papers have been published in the field of binary stars using many astronomical methods to calculate the orbital and physical parameters of those stars, such as, for example, the method of Tokovinin, the Docobo geometrical methods, and the Al-wardat method as a complementary atmospheric modeling method (J. Docobo et al. 1988; A. Tokovinin 1992a, 1992b; J. Docobo et al. 2000; M. A. Al-Wardat 2007, 2009).

1.4 Observational Techniques and Types of Binaries

Astrometric, spectroscopic, and eclipsing binaries are the main types of binary systems. It is challenging to determine the individual masses of a system using a single technique. Fifty years ago, speckle interferometry entered the field of observing binary stars effectively and accurately, and it has become a significant part of the observational processes employed by researchers around the

Table 1: Parameters of systems.

Property	HD 130669	HD 184467	HD 191854	HD 214222	Source of data
α_{2000}	$14^h 49^m 13^s.62$	$19^h 31^m 07^s.96$	$20^h 10^m 13^s.32$	$22^h 35^m 42^s.67$	(M. Wenger et al. 2000)
δ_{2000}	$+10^\circ 12' 52''.06$	$+58^\circ 35' 09''.60$	$+43^\circ 56' 44''.07$	$+53^\circ 12' 14''.41$	(M. Wenger et al. 2000)
m_V [mag]	8.42	6.59	7.606	8.036	(Esa 1997)
π_{Hip1} [mas]	-	59.84 ± 0.64	19.45 ± 0.80	13.76 ± 0.79	(F. van Leeuwen 2007)
π_{Hip2} [mas]	22.59 ± 1.23	58.96 ± 0.65	19.48 ± 0.54	14.15 ± 0.74	(M. Perryman et al. 1997)
π_{Gaia1} [mas]	-	58.37 ± 0.54	-	46.61 ± 0.83	(A.G. Brown et al. 2016)
π_{Gaia2} [mas]	-	54.8715 ± 0.24	19.2965 ± 0.1282	14.235 ± 0.319	(Gaia Collaboration et al. 2018b)
π_{Gaia3} [mas]	-	52.2767 ± 0.3519	-	-	(Gaia Collaboration et al. 2021)

* <http://simbad.u-strasbg.fr/simbad/sim-fid>.

world (A. Labeyrie 1970; H. A. McAlister 1976, 1977, 1978; I. Balega et al. 1984; D. Bonneau et al. 1986; A. Abushattal et al. 2022a). Two types of binary systems correlate with the masses of the components of the binary star: the astrometric binary (AB) and the double-lined spectroscopic binary (SB2). In AB, the orbit solution is determined via the parallax, and by applying Kepler’s third law, we can determine the total mass of the system. In the SB2 orbital solution, we can determine the mass ratio of the components, and by combining both methods, we can determine the three-dimensional orbit, the individual masses, and the orbital parallax. Measuring the orbital parallax is considered an effective verification method for astrometric parallaxes after systematic errors were found in the Gaia data release (Gaia DR2) for bright stars (K. G. Stassun & G. Torres 2018; R. Drimmel et al. 2019; E. Vasiliev 2019; A. Abushattal et al. 2022b). During recent years, there have been many publications that relied on such a research method to determine the physical parameters with a combination of each technique (J. A. Docobo et al. 2014, 2018c; X.-L. Wang et al. 2016; J. A. Docobo et al. 2017; K. V. Lester et al. 2019a, 2019b, 2020; L. Piccotti et al. 2020). Precision astrometric interferometry in binary star systems is a promising technique for planet searches that complements the radial-velocity method that has been so successful. Internal errors of a few microarcseconds are possible if the systematic errors can be controlled (J. T. Armstrong et al. 2004).

1.5 Binary Systems and Exoplanet Habitability

Main-sequence and pre-main-sequence stars constitute approximately 50% of multiple-star systems, positioning binary systems as favorable environments for exoplanet exploration by space missions such as CoRoT, Kepler, K2, and TESS, intending to identify Earth-like planets (G. R. Ricker et al. 2010; S. Eggl et al. 2012; W. J. Borucki 2016; A. Abushattal et al. 2019; S. B. Howell et al. 2021). Multiple stars often contain the most massive exoplanets, and binary stars are among the most important hosts of giant exoplanets in multiple systems (C. Fontanive and D. Bardalez Gagliuffi 2021). A couple of important features in the study of exoplanets are the potential habitability of a planet and its orbital stability, which both depend on the parameters of the host binary star. Such parameters are the individual masses, the semimajor axis, the orbital eccentricity, the luminosities, and temperatures, and they are the main target of this work (K.-U. Michel & M. Mugrauer 2021; E. Pilat-Lohinger and A. Bazso 2021; N. Georgakarakos and S. Eggl 2019).

The key idea of this work is to combine the high-grade visual solution with a definitive spectroscopic orbital solution for selected double-lined spectroscopic candidates to calculate the orbital parallax and the individual masses. Also, we estimate the atmospheric and fundamental parameters of the individual components. First, these results will be compared with other values resulting from the use of different methods, such as Edwards’s method (T. Edwards 1976; A. A. M. Abushattal 2017) or Al-Wardat’s method for analyzing binary and multiple stars (M. A. Al-Wardat 2002, 2012). Second, we will use these results to describe the three-dimensional orbits for each system. Third,

these quantities, together with the luminosities (e) and temperatures (T), will be used to assess the potential of planetary habitability and orbital stability. Finally, we will use our results to determine the minimum size of the telescope necessary to visually observe these systems (A. A. M. Abushattal 2017; A. A. Abushattal et al. 2019b).

1.6 Al-Wardat’s Method Description and Validation

Al-Wardat’s method for analyzing stellar systems is a computational method that utilizes the observed photometry and spectral energy distributions (SEDs) of entire stellar systems to build synthetic SEDs for the individual components of the systems. These systems are barely resolved using space telescopes or special techniques on ground-based telescopes. The method constructs synthetic SEDs for the individual components or variability phases through an iterative process. The results are used for estimating the physical parameters of these component, from which their masses, spectral types, luminosity classes, and populations are defined. The method uses local thermodynamical equilibrium plane-parallel model atmospheres, typically using Kurucz ATLAS 12 models, to generate the synthetic SED for each component. The method was successfully used to analyze 10s of binary and multiple stellar systems, as well as some variable stars (M. Al-Wardat 2002a, 2008, 2009, 2012; M. A. Al-Wardat et al. 2016, 2017a; S. G. Masda et al. 2018, 2019b; A. M. Hussein et al. 2022; A. A. Abushattal et al. 2024).

1.7 Objectives and Structure

In this study, we combine visual and spectroscopic data to determine the fundamental physical and orbital parameters of four Sun-like double-lined spectroscopic binary systems. To resolve astrometric discrepancies, Al-Wardat’s atmospheric modeling method is applied to derive precise stellar masses, orbital parallaxes, and other essential parameters. The habitability and orbital stability of hypothetical planets around these systems are also assessed. This paper is organized as follows: Section 2 outlines data sources and selection criteria, Section 3 presents orbital analysis, Section 4 presents atmospheric modeling techniques, Section 5 discusses mass and parallax determinations, Section 6 examines habitability and stability conditions, and Section 7 summarizes our findings and their implications for the future.

2 Data Resources and Selection of Candidates

The binary systems HD 130669, HD 184467, HD 191854, and HD 214222 were chosen based on stringent criteria to ensure the robustness of our analysis. First, each system is classified into a double-lined spectroscopic binary (SB 2) in the ninth catalog of spectroscopic binary orbits (SB9), which provides information on mass ratios. Additionally, all systems feature high-quality visual orbital solutions from the Sixth Catalog of Visual Binary Star Orbits, which enables combined spectroscopic and visual analysis. Additionally, we prioritized systems with well-graded orbits (grade 1 or 2 for visual orbits and grade 5 for spectroscopic orbits; J. Docobo et al. 2018). This ensured data reliability. Furthermore, the systems were selected for their Sun-like characteristics, including F-, G-, or K-type main-sequence components, which makes them suitable candidates for the study of planetary habitability. This work focuses on binary stars that possess both spectroscopic and visual orbits, combining the two types into one known as a spectroscopic-visual binary. In the Ninth Catalog of Orbits of Spectroscopic Binaries (SB9), we first look for double-lined spectroscopic binary candidates. These types of binaries are essential for such studies because they provide an important piece of information: the mass ratio of the binary components. The first source, SB9, is a catalog of

the orbital elements of spectroscopic binary stars, accessible online at <https://sb9.astro.ulb.ac.be/>. It contains valuable information about identified selected samples, which can be separated into basic data (coordinates, spectral types, and apparent magnitudes) and identifiers using common catalogs (HD, HIP, BD). The most important part is the orbital solution, which contains the orbital elements with errors, derived quantities, and the grade of the orbits (1: poor, 5: definitive) with references (D. Pourbaix et al. 2004). The second source is the Sixth Catalog of Orbits of Visual Binary Stars, which can be accessed online at <http://www.astro.gsu.edu/wds/orb6.html>. It includes 3318 systems with 10,089 orbits graded on a scale of 1 to 5 (1: definitive, 5: poor). On the website, one can find an introduction, the Orbit grading method, and a description of the catalog (orbital elements, ephemerides, notes, references). Thus we search for SB2s with reliable visual and spectroscopic orbital solutions. This is achieved by combining data from the sixth catalog with that from SB9 to obtain the appropriate primary data for such a study.

3 Visual and Spectroscopic orbits

The systems we investigate in the work are as follows:

HD 130669, A 2983, HIP 72479. In 1955, N. G. Roman listed HD 130669 in the Catalogue of High-velocity Stars as a K2V star, with a spectroscopic orbit of $0''.0275$ and photoelectric magnitudes and a color index of $V = 8.43$ and $B - V = 0.88$ (N. G. Roman 1955). O. J. Eggen calculated the dynamical parallax of this system to be $0''.022$, based on a period of 10 yr, with a spectral type of G9 V. Five years later, he revised it to be $0''.025$, and R. F. Griffin suggested a spectral type of K0V (O. J. Eggen 1955; R. F. Griffin 2015). Unfortunately, in the SIMBAD database, this system doesn't have a Gaia parallax, while Hipparcos calculates it to be $0''.02259$, with a photometry of $V = 8.42$ and $B - V = 0.866$ (E. Hog et al. 2000). R. F. Griffin published the orbital solution of the system in 2015 based on 51 observations, all of which were determined at the 36-inch observatory at Cambridge University (R. F. Griffin 2015).

The director of Ramon Maria Aller Observatory, J. A. Docobo, published a practical analytic method to determine the orbital solution for binary systems. This method calculates the best orbit of the system that passes through three base points with a best fit (J. A. Docobo 1985, 2012). In 2014, he published an important method that allows for the determination of the orbits of spectroscopic binaries with an astrometric observation (J. A. Docobo et al. 2014). Furthermore, this method is considered an effective way to improve the previous orbital solutions and analyze the consistency of the astrometric observations. The best orbit is selected based on the better rms values in θ and ρ with high coherence with the common orbital elements from the spectroscopic solution. The new astrometric orbital elements for HD 130669 are listed in Table 2.

HD 184467, Hip 95995, Gliese 762.1. The visual observations for this system began by Harold A. McAlister at the Kitt Peak National Observatory (KPNO) in 1983. He used a speckle interferometry of a 4 m telescope (H. McAlister et al. 1983). In SIMBAD, this system has been classified as a main-sequence one with a spectral type of K2 (P. C. Keenan and R. C. McNeil 1989). In 2010, Farrington used the CHARA Array to determine the combination of visual-spectroscopic solutions. He suggested this system to be an SB 2 with a $K2V + K4V$ spectral type for each component with an apparent magnitude ($mv = 6.59$) and a period of about 494 days (C. D. Farrington et al. 2010). M Suhail estimated the first solution using Al-Wardat's complex method as a close visual-spectroscopic binary. He presents the individual physical and geometrical parameters for each system component. The evolutionary tracks showed the masses to be between 0.8 and 0.9 solar masses for both components as main-sequence stars with K0V and K1.5V. Isochrones showed this system with an age of around 9 ± 1 Gyr as low -and intermediate- mass stars, with a magnitude

difference (Δm) of 0.26 ± 0.03 (S. G. Masda et al. 2016). In 2017, F. Kiefer observed this system using the spectrograph of the Observatoire de Haute-Provence (SOPHIE) and then combined the radial-velocity measurements with the astrometric measurements. He estimated the masses of each component to be $MA = 0.833 \pm 0.031$ and $MB = 0.812 \pm 0.030$, with a parallax of 56.10 ± 0.81 mas and with an absolute magnitude of 5.98 ± 0.02 for the primary component and 6.24 ± 0.03 mag for the secondary component (F. Kiefer et al. 2018). In 2021, Mitrofanova, using the radial-velocity amplitudes method, calculated the individual masses for HIP 95995 to be $MA = 0.99 \pm 0.11$ and $MB = 0.36 \pm 0.11$ (A. Mitrofanova et al. 2021).

HD 191854, ADS 13461, HIP 99376. This system has apparent and absolute magnitudes of $V = 7.43$ and $MV = 4.3$, respectively, with $B - V = 0.66$, where the difference in magnitude (Δm) is 0.74, and a parallax of 0.018 mas (O. Eggen 1965). In 1969, James W. Christy and R. L. Walker classified this system as a G5 main-sequence star with a G4V spectral type for the main component and as a G8V for the second component, with a difference in magnitude of $\Delta m = 0.5$ (J. W. Christy and R. Walker 1969). W. D. Heintz gave the absolute magnitudes of the system components to be 8.3 and 9.0 with a spectral type of G4V and an orbital period of 85.61 days, a semimajor axis of $0''.449$, an eccentricity of 0.488, an inclination of 116.4, and a dynamical parallax of 0.019 mas (W. Heintz 1997). In 2000, D. Pourbaix described the spectral type of both system components as G4V and G8V. The apparent magnitudes of the system were 8.058 and 8.598, with a mass of 1.2 and 0.9 solar masses. The spectroscopic orbital parameters are listed in Table 3 ($P = 85.2$, $T = 1970.1$, $a = 0.458$, $e = 0.492$, $i = 115^\circ.3$, $\omega = 159^\circ$, $\Omega = 321^\circ.7$; D. Pourbaix 2000).

HD 214222, ADS 16098, HIP 111528. This is a spectroscopic binary with an apparent magnitude of 8.4 and spectral type of G0V, with a mass of 1.22 solar masses for component A and 1.16 solar masses for component B. The orbital solution can be found in Table 3 (D. Pourbaix 2000). G. Starikova suggested that ADS 16098 has a total mass of 1.9 solar masses, 0.95 for each component. She also suggested an orbital period of 22.18 yr, a semimajor axis of $0''.150$, and a parallax of $0''.015$ (G. Starikova 1978). T. Edwards described the Morgan–Keenan (MK) classification of this system as G1 for both components with a difference in magnitude of 0.1 and an apparent magnitude of 8.5 (T. Edwards 1976). E. P. Horch et al. (2015) determined that the spectral types of the components are G2V and G3V, with individual masses of 1.00 and 0.97 solar masses, respectively (see Table 3).

Table 2: Visual orbital elements.

Element	HD 130669	HD 184467	HD 1918154	HD 214222
P (yr)	10.01	494.307 ± 0.012	85.61	22.3455 ± 0.000
T	2018.174	2013.75	1999.85	1985.246 ± 0.000
e	0.518	0.38933 ± 0.00029	0.488	0.362 ± 0.000
a ($''$)	0.123	0.081 ± 0.000	0.449	0.1446 ± 0.000
i ($^\circ$)	43.5	146.15 ± 0.46	116.4	63.3 ± 0.3
Ω ($^\circ$)	144.8	245.72 ± 0.13	142.2	110.5 ± 0.3
ω ($^\circ$)	335.9	180.325 ± 0.041	339.4	144.2 ± 0.0
Reference	(J. Docobo et al. 2018)	(F. Kiefer et al. 2018)	(W. Heintz1 1997)	(E. P. Horch et al. 2015)
Grade*	1	1	2	2

*Sixth Catalog of Orbits of Visual Binary Stars (1: definitive, 5: poor).

4 Atmospheric and Fundamental Parameters

In this section, we study the four systems using Al-Wardat’s method for analyzing binary and multiple systems (M. Al-Wardat 2002b; M. A. Al-Wardat 2012). This computational spectrophotometric method uses Kurucz Atlas9 line-blanketed plane-parallel model atmospheres of single stars to build the entire SEDs of the binary and multiple systems. Hence this synthetic photometry method cal-

Table 3: Spectroscopic orbital elements.

Element	HD 130669	HD 184467	HD 191854	HD 214222
P (d)	3619.0 ± 66.0	494.313 ± 0.012	3619.0 ± 66.0	8161.68 ± 40.1766
P (yr)	9.915 ± 0.005	1.3534 ± 0.0001	85.215 ± 0.181	22.346 ± 0.110
T (MJD)	54513.0 ± 11.0	56549.487 ± 0.046	40476.9 ± 63.76	46155.7 ± 35.4242
K ₁ (km/s)	6.73 ± 0.07	9.4911 ± 0.0026	3.9737 ± 0.44	6.3964 ± 0.14
K ₂ (km/s)	6.76 ± 0.09	9.733 ± 0.026	5.1183 ± 0.47	6.73626 ± 0.13
e	0.488 ± 0.009	0.38926 ± 0.00030	0.4922 ± 0.0033	0.36168 ± 0.013
ω_1 (°)	163.0 ± 2.0	180.300 ± 0.043	338.93 ± 1.00	144.22 ± 2.2
$a_1 \sin i$ (Gm)	293 ± 6	59.424 ± 0.015	1480.46 ± 160.00	669.279 ± 15.00
$a_2 \sin i$ (Gm)	294 ± 7	60.94 ± 0.16	1906.86 ± 180.00	704.837 ± 15.00
$a \sin i$ (Gm)	587 ± 9.2	120.36 ± 0.16	3387.32 ± 240.8	1374.112 ± 22.10
$\mathcal{M}_1 \sin^3 i$ (M _⊙)	0.308 ± 0.012	0.14399 ± 0.00076	0.9034 ± 0.2000	0.79917 ± 0.038
$\mathcal{M}_2 \sin^3 i$ (M _⊙)	0.306 ± 0.011	0.14041 ± 0.00038	0.7014 ± 0.1600	0.75885 ± 0.038
q	1.007 ± 0.016	1.0255 ± 0.0011	1.288 ± 0.3200	1.0531 ± 0.016
References	(R. F. Griffin 2012)	(F. Kiefer 2018)	(D. Pourbaix 2000)	(D. Pourbaix 2000)
Grade*	5	5	5	5

* The ninth catalogue of spectroscopic binary orbits (1: poor, 5: definitive).

culates their synthetic magnitudes and color indices. The data required to apply this technique are the magnitude differences obtained either from speckle interferometry measurements or from spectroscopic measurements, visual magnitude, and color indices. These data are widely accessible; therefore, the technique can be used to study the properties of all binary and multiple systems, including face-on orbit binaries. This method can be used even without the system’s orbital information and spectroscopic data, and that makes it an ideal technique to study the properties of the systems under investigation. The method was used to analyze several binary and multiple systems and estimate their complete set of atmospheric and fundamental parameters of individual components (e.g., M. Al-Wardat 2007, M. Al-Wardat and H. Widyan 2009, M. Al-Wardat 2009, M. Al-Wardat 2012, M. Al-Wardat et al. 2014a, M. Al-Wardat et al. 2014b, M. A. Al-Wardat et al. 2016, S. G. Masda et al. 2016, M. Al-Wardat et al. 2017b, S. G. Masda et al. 2018, S. Masda et al. 2019a, M. A. Al-Wardat et al. 2021a, Y. M. Al-Tawalbeh et al. 2021, Z. T. Yousef et al. 2021, and M. A. Al-Wardat et al. 2021b).

We now apply the method to each of our systems.

HD 130669, A 2983, HIP 72479. Having a 0.09 magnitude difference and using the orbital parallax from this work, Al-Wardat’s method provides an estimate for the synthetic SEDs of the entire system and individual components of HD 130669, as shown in Figure 1. The calculated magnitudes and color indices of the synthetic SED for the entire system and individual components of HD 130669 are listed in Table 4. The estimated atmospheric and fundamental parameters are listed in Table 5. The effective temperature and luminosity are used to locate the positions of the components on the evolutionary tracks of L. Girardi et al. (2000), where the metallicity used was $Z = 0.019$ based on the measured iron abundance relative to the Sun $Fe/H = -0.03$ (C. Soubiran et al. 2016). The evolutionary tracks of the system using Al-Wardat’s method results are shown in Figure 5. The low mass of the system did not allow for the estimation of the age of the system.

HD 184467, Hip 95995. Using Al-Wardat’s method, the synthetic SEDs of the combined and individual components of HD 184467 are estimated and shown in Figure 2. The calculated magnitudes and color indices of the synthetic SEDs of the combined and individual components of HD 184467 are listed in Table 4. The estimated atmospheric and fundamental parameters are listed in Table 5. The effective temperature and luminosity are used to locate the positions of the components on the evolutionary tracks of L. Girardi et al. (2000), where the metallicity used was $Z = 0.008$ based on the measured iron abundance relative to the Sun $Fe/H = -0.25 \pm 0.006$ (M. Netopil 2017). Using Al-Wardat’s method results, the evolutionary tracks of the system are shown in Figure 5. The best

Table 4
Magnitudes and Color Indices of the Entire Synthetic Spectrum and Individual Components

	Johnson							Strömgren						Tycho			
	<i>U</i>	<i>B</i>	<i>V</i>	<i>R</i>	<i>U - B</i>	<i>B - V</i>	<i>V - R</i>	<i>u</i>	<i>v</i>	<i>b</i>	<i>y</i>	<i>u - v</i>	<i>u - b</i>	<i>b - y</i>	<i>B_T</i>	<i>V_T</i>	<i>B_T - V_T</i>
HD 130669																	
E	9.78	9.28	8.42	7.95	0.50	0.864	0.47	10.94	9.76	8.88	8.38	1.18	0.88	0.50	9.52	8.51	1.01
A	10.46	9.98	9.13	8.67	0.48	0.85	0.46	11.62	10.45	9.58	9.09	1.17	0.87	0.49	10.21	9.22	0.99
B	10.62	10.09	9.22	8.74	0.52	0.87	0.48	11.78	10.56	9.68	9.17	1.19	0.90	0.50	10.33	9.31	1.02
HD 184467																	
E	7.95	7.46	6.60	6.13	0.49	0.86	0.47	9.11	7.93	7.05	6.56	1.17	0.88	0.49	7.69	6.69	1.0
A	8.49	8.04	7.20	6.75	0.45	0.83	0.45	9.64	8.50	7.64	7.16	1.14	0.85	0.48	8.27	7.29	0.97
B	8.97	8.41	7.53	7.04	0.55	0.89	0.49	10.14	8.92	7.99	7.48	1.22	0.92	0.51	7.74	7.16	0.57
HD 191854																	
E	8.26	8.07	7.40	7.04	0.18	0.670	0.36	9.40	8.43	7.77	7.37	0.97	0.66	0.40	8.24	7.47	0.76
A	8.40	8.25	7.61	7.26	0.15	0.64	0.35	9.55	8.59	7.97	7.58	0.95	0.63	0.39	8.41	7.68	0.73
B	10.50	10.12	9.31	8.88	0.39	0.80	0.43	11.65	10.55	9.75	9.28	1.09	0.81	0.47	10.33	9.40	0.93
HD 214222																	
E	8.85	8.73	8.19	7.79	0.12	0.610	0.33	9.99	9.06	8.46	8.09	0.94	0.60	0.37	8.87	8.19	0.69
A	9.51	9.40	8.80	8.47	0.10	0.59	0.33	10.66	9.73	9.14	8.77	0.93	0.59	0.37	9.55	8.87	0.68
B	9.70	9.57	8.95	8.61	0.13	0.62	0.34	10.85	9.91	9.30	8.92	0.94	0.61	0.38	9.72	9.02	0.70

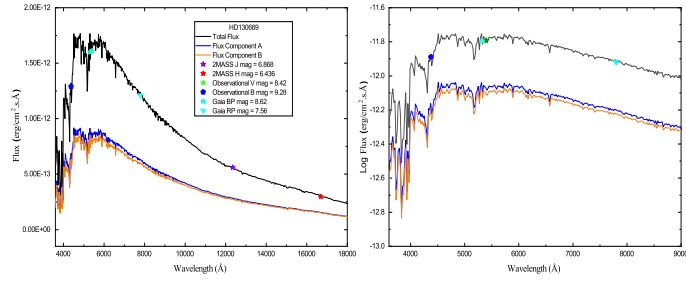


Figure 1: Synthetic spectral energy distribution (SED) of the binary system HD 130669 constructed using Al-Wardat’s complex method and Kurucz’s ATLAS9 model atmospheres. The total flux (black), flux of component A (blue), and flux of component B (orange) are shown. Overplotted are observed photometric fluxes from 2MASS (J, H), Gaia (BP, RP), and Johnson photometry (B, V) with their respective magnitudes. This comparison validates the consistency between the synthetic model and observed data across a wide wavelength range (3,500 – 18,000Å).

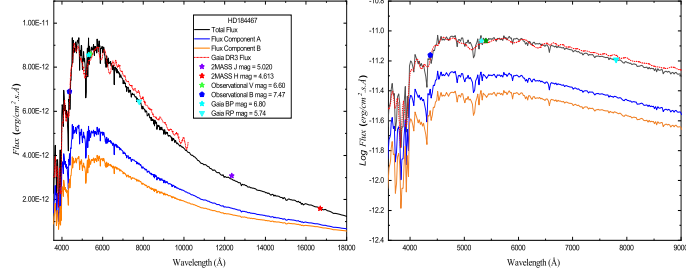


Figure 2: Synthetic spectral energy distribution (SED) of the binary system HD 184467 constructed using Al-Wardat’s complex method and Kurucz’s ATLAS9 model atmospheres. The total flux (black), flux of component A (blue), and flux of component B (orange) are shown. Overplotted are observed photometric fluxes from 2MASS (J, H), Gaia (BP, RP), and Johnson photometry (B, V) with their respective magnitudes. This comparison validates the consistency between the synthetic model and observed data across a wide wavelength range (3,500 – 18,000Å).

estimate for the age of the system is 6.3 Gyr isochrone for both components. This suggests that fragmentation is the most probable formation mechanism of the system.

HD 191854. Again, using Al-Wardat’s method, we derive the synthetic SEDs of the combined and individual components of HD 191854. These are shown in Figure 3. The calculated magnitudes and color indices of the synthetic SEDs of the combined and individual components of HD 191854 are listed in Table 4, and the estimated atmospheric and fundamental parameters are listed in Table 5. The effective temperatures and luminosities of the components were used to place them on the evolutionary tracks of L. Girardi et al. (2000), with a metallicity of $Z = 0.004$, corresponding to a measured iron abundance of $Fe/H = -0.05$ (M. Netopil 2017). As shown in Figure 5 and determined using the results of Al-Wardat’s method, the best-fit isochrone indicates an estimated system age of approximately 6.3 Gyr for both stars. This finding supports the likelihood that the system formed through a fragmentation process.

HD 214222. As we did with the rest of the systems, we provide the synthetic SEDs for HD 214222, which can be seen in Figure 4. The calculated magnitudes and color indices of the synthetic can be found in Table 4, while the estimated atmospheric and fundamental parameters are listed in Table 5. The effective temperature and luminosity of the components were used to place them on the evolutionary tracks of L. Girardi et al. (2000), adopting a metallicity of $Z = 0.019$, which corresponds to a measured iron abundance of $[Fe/H] = -0.05$ (A. Gáspár et al. 2016). As illustrated in Figure 5 and based on Al-Wardat’s method, the best-fitting isochrone indicates an age of approximately 3.548 Gyr for both components. This result suggests that the system most likely formed through the fragmentation mechanism.

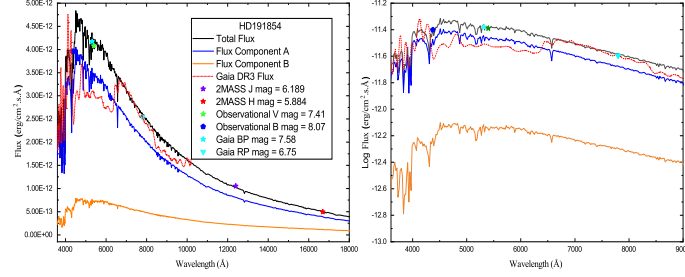


Figure 3: Synthetic spectral energy distribution (SED) of the binary system HD 191854 constructed using Al-Wardat’s complex method and Kurucz’s ATLAS9 model atmospheres. The total flux (black), flux of component A (blue), and flux of component B (orange) are shown. Overplotted are observed photometric fluxes from 2MASS (J, H), Gaia (BP, RP), and Johnson photometry (B, V) with their respective magnitudes. This comparison validates the consistency between the synthetic model and observed data across a wide wavelength range (3,500 – 18,000Å).

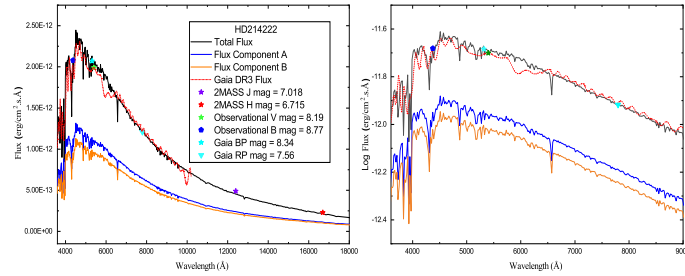


Figure 4: Synthetic spectral energy distribution (SED) of the binary system HD 21422 constructed using Al-Wardat’s complex method and Kurucz’s ATLAS9 model atmospheres. The total flux (black), flux of component A (blue), and flux of component B (orange) are shown. Overplotted are observed photometric fluxes from 2MASS (J, H), Gaia (BP, RP), and Johnson photometry (B, V) with their respective magnitudes. This comparison validates the consistency between the synthetic model and observed data across a wide wavelength range (3,500 – 18,000Å).

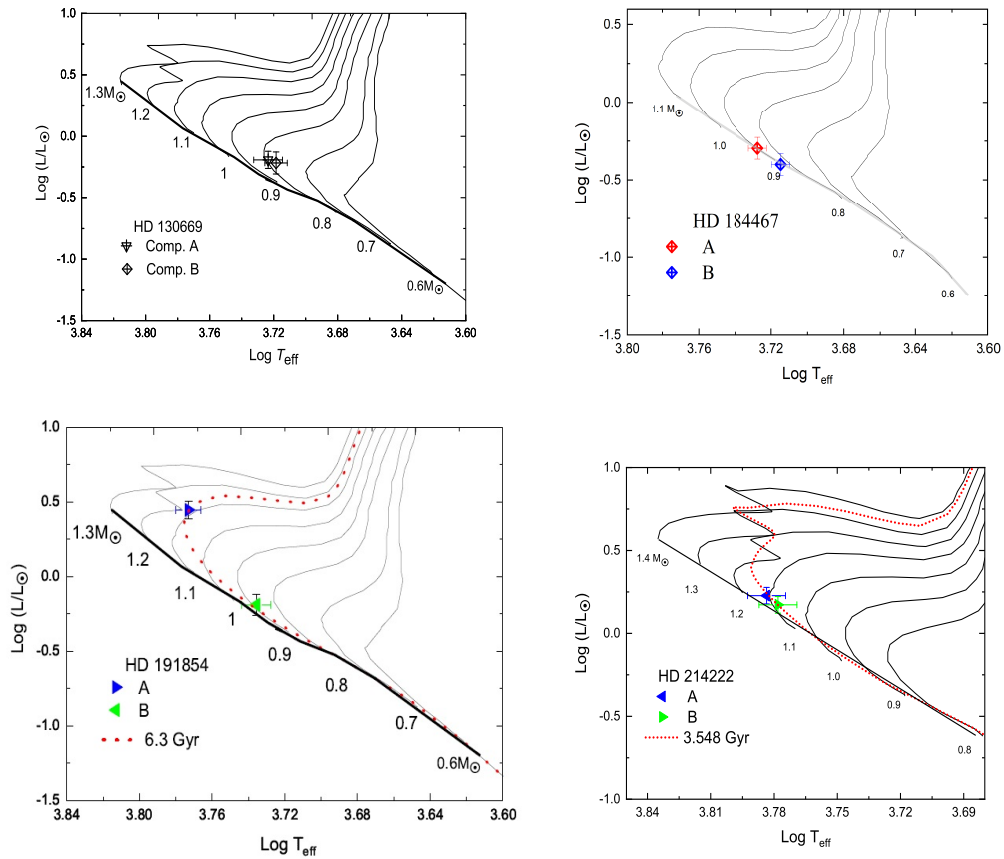


Figure 5: H–R diagrams for the binary systems HD 130669, HD 184467, HD 191854, and HD 214222. The positions of the individual stellar components (A and B) are plotted with their respective uncertainties. Evolutionary tracks corresponding to different stellar masses are shown by black lines, while the system’s best-fitting isochrone (age) is indicated by a red dotted line. The Zero-Age Main Sequence (ZAMS) is depicted as a thick solid black line. These diagrams were constructed using the evolutionary models to determine the masses and ages of the components based on their effective temperatures and luminosities.

Table 5
The Fundamental Parameters of the Individual Components of the Systems as Estimated Using Al-Wardat's Method

Comp.	T_{eff} K	R, R_{\odot}	$\log g, \text{cm/s}^2$	L, L_{\odot}	M_{bol} mag	M_V mag	$\mathcal{M}, \mathcal{M}_{\odot}$	Sp	Age. Gyr
HD 130669									
A	5290	0.956	4.40	0.64	5.23	5.4	0.89	K0V	
B	5230	0.95	4.40	0.61	5.29	5.55	0.88	K0V	
HD 184467									
A	5340	0.832	4.60	0.51	5.49	5.70	0.91	G9 V	Zero- age
B	5185	0.783	4.60	0.39	5.75	6.01	0.85	K1V	
HD 191854									
A	5930	1.585	4.8	2.79	3.64	3.73	1.12	G0V	6.3
B	5440	0.906	4.47	0.65	5.25	5.40	0.89	G8V	6.3
HD 214222									
A	6075	1.14	4.37	1.59	4.25	4.32	1.12	F9V	2.818
B	6000	1.095	4.39	1.40	4.39	4.46	1.09	F9V	2.818

5 Parallax and Masses

By studying double-lined spectroscopic binaries, we can accurately determine stellar masses and orbital parameters. We can calculate the entire orbital geometry by combining spectroscopic radial-velocity measurements with visual or interferometric orbit measurements, including the inclination and mass ratio. Thus absolute masses can be determined without the ambiguity of spectroscopic data alone. By combining angular and linear orbital measurements, orbital parallax can be calculated, offering a direct and reliable method to determine stellar distances. This approach also helps validate and refine astrometric catalogs like Hipparcos and Gaia. Then, by combining synthetic photometry with modeling of how energy is distributed across different wavelengths, this method allows for a detailed understanding of the two stars in a binary system. This understanding is from both a physical and atmospheric perspective. This means that using spectroscopic and visual methods together is a strong and accurate way to study SB2 systems. This can help us improve models of how stars evolve and advance our understanding of stellar astrophysics.

We can calculate the total mass of the system using Kepler's third law:

$$\mathcal{M}_1 + \mathcal{M}_2 = \left(\frac{a''}{\pi''} \right)^3 \frac{1}{P^2}, \quad (1)$$

where \mathcal{M}_1 and \mathcal{M}_2 are the masses of the two stars, a is the semimajor axis in arcseconds, P is the period in years, and π is the Gaia parallax. Also, we can obtain the mass ratio for the double-lined spectroscopic binaries from the orbital solution using

$$q = \frac{\mathcal{M}_1 \sin^3(i)}{\mathcal{M}_2 \sin^3(i)} = \frac{\mathcal{M}_1}{\mathcal{M}_2} \quad (2)$$

where i is the inclination in degrees. Then, by using equations (1) and (2), we can determine the most precise individual mass of each component:

$$\mathcal{M}_1 = q * \mathcal{M}_2, \quad (3)$$

$$\mathcal{M}_2 = \left(\frac{a''}{\pi''}\right)^3 \left(\frac{1}{P}\right)^2 \left(\frac{1}{1+q}\right). \quad (4)$$

Considering $A = a \sin i$, $A_1 = a_1 \sin i$, $A_2 = a_2 \sin i$

$$A_{a.u.} = \frac{(A_1 + A_2)_{km}}{149597870.700}. \quad (5)$$

Stellar masses are influenced significantly by uncertainties in orbital inclination (i) and orbital parallax (π). Based on the angular semi-major axis and parallax, the physical semi-major axis can be calculated as follows:

$$\pi = \frac{a''}{a}. \quad (6)$$

By adding the a^3 term to Kepler's third law, even small parallax errors are magnified, resulting in greater mass uncertainty. Furthermore, Kepler's third law includes a triple dependence term, which magnifies even small errors in parallax, thus increasing mass uncertainty. Nonlinear errors can also occur due to deviations in inclination, especially when orbits are not edge-on. As shown in Table 6, we propagated these uncertainties using standard partial derivative-based error propagation methods. Therefore, deviations in inclination, especially for orbits that are not edge-on, can cause nonlinear errors in mass estimations. We apply the previous equations to determine the individual masses and orbital parallax of the double-lined spectroscopic binary HD 184467.

HD 184467, ADS 13529, HIP 96295. We apply the same combined methodology of visual and spectroscopic analysis to the system HD 184467 in order to determine its parallax and individual stellar masses. Using the orbital solution and inclination angle from the visual orbit ($i = 146^\circ.15 \pm 1^\circ.5$), and calculating $a \sin i$ from the spectroscopic orbit, we find the semimajor axis of the system to be $a = 1.444 \pm 0.0042$ au.

The visual orbit provides an angular semimajor axis of $a'' = 0''.081 \pm 0''.001$. From this, we calculate the orbital parallax using

$$\pi_{\text{orb}} = \frac{a''}{a} = \frac{0.081}{1.444} = 0''.05610 \pm 0''.00071,$$

which corresponds to a distance of approximately 17.82 pc. This is in excellent agreement with the orbital parallax provided in the orbital solution and confirms the precision of the combined visual-spectroscopic model.

Using Kepler's third law with this parallax and the orbital period $P = 1.3537$ years, we determine the total mass of the system to be

$$\mathcal{M}_{\text{total}} = \left(\frac{a''}{\pi''}\right)^3 \cdot \frac{1}{P^2} = \left(\frac{0.081}{0.05610}\right)^3 \cdot \frac{1}{(1.3537)^2} = 1.6451 \mathcal{M}_\odot.$$

From the spectroscopic mass ratio $q = \mathcal{M}_1/\mathcal{M}_2 = 1.0254$, we derive the individual component masses:

$$\begin{aligned} \mathcal{M}_2 &= \frac{\mathcal{M}_{\text{total}}}{1+q} = \frac{1.6451}{1+1.0254} = 0.8122 \pm 0.0107 \mathcal{M}_\odot, \\ \mathcal{M}_1 &= q \cdot \mathcal{M}_2 = 1.0254 \times 0.8122 = 0.8329 \pm 0.0188 \mathcal{M}_\odot. \end{aligned}$$

These results are in strong agreement with Al-Wardat's method, which yields

$$\mathcal{M}_1 = 0.91 \pm 0.05 \mathcal{M}_\odot, \quad \mathcal{M}_2 = 0.85 \pm 0.04 \mathcal{M}_\odot.$$

This consistency between orbital dynamics and atmosphere modeling confirms the reliability of the adopted method.

The dynamical parallax based on Al-Wardat’s masses and the orbital elements is:

$$\pi_{\text{dyn}} = 0''.05630 \pm 0''.0016,$$

The close match between the orbital, dynamical, and catalogue parallaxes demonstrates the strength of the combined approach for accurately characterizing SB2 systems.

HD 130669, A 2983, HIP 72479: The V magnitude of HD 130669, as provided by SIMBAD, is 8.42, with $B - V = 0.866$ (M. Perryman et al. 1997; F. van Leeuwen 2007). We apply the same methodology for HD 130669 and we estimate the difference in magnitudes to be 0.5, which agrees with Griffin’s suggestion (M. Al-Wardat 2012; R. F. Griffin 2015). The total absolute magnitude equals 5.19 ± 0.04 , while the absolute magnitudes for the components are 5.00 ± 0.02 and 5.50 ± 0.02 , respectively. R. F. Griffin (2015) suggests K0V spectral types for both components with 2-3 subtypes in the accuracy. The total mass is 1.92 ± 0.09 , which is close to 1.85 ± 0.08 (of this work). The mass ratio is 1.03 ± 0.034 , which is in good agreement with Griffin’s calculation of 1.005 ± 0.016 (R. F. Griffin 2015). The inclination is equal to $42.48^\circ \pm 2.1^\circ$, which is very close to $43.5^\circ \pm 0^\circ$ of this work.

M. Al-Wardat (2012) analyzed the system using the Hipparcos 1 parallax and estimated the masses of the individual components to be:

$$\mathcal{M}_1 = 0.94 \pm 0.05 \mathcal{M}_\odot \text{ and } \mathcal{M}_2 = 0.85 \pm 0.04 \mathcal{M}_\odot. \quad (7)$$

M. Al-Wardat (2012) used a 0.5 magnitude difference from speckle interferometry. The speckle magnitude difference gives a mass ratio of about 1.10, different from the spectroscopic mass ratio of 0.9 in Esa (1997), which gives a 0.2 difference in the mass ratio.

Here, we take the same steps to determine $a \sin i$ in au, and the visual orbit inclination $i = 43.5^\circ \pm 0^\circ$. This yields a semimajor axis $a = 5.7003 \pm 0.0615$ au. Combining this result with the semimajor axis of 0.123 ± 0.000 arcseconds from the visual solution, we can then deduce the orbital parallax of the system to be $\pi_{\text{orb}} = 0.0216'' \pm 0.0015''$, which agrees with the Hipparcos parallax of $0.02259'' \pm 0.00125''$ (F. van Leeuwen 2007). Using this new parallax, the total mass is $\mathcal{M}_{\text{total}} = 1.8486 \pm 0.0815 \mathcal{M}_\odot$. Hence, using the spectroscopic solution, the mass ratio and the individual masses of the system are $q = 1.005 \pm 0.016$, $\mathcal{M}_1 = 0.9266 \pm 0.0511 \mathcal{M}_\odot$ and $\mathcal{M}_2 = 0.9220 \pm 0.0448 \mathcal{M}_\odot$ respectively. On the other hand, using Al-Wardat’s method, we find for the total mass and the individual masses of the system $q = 1.01 \pm 0.016$, $\mathcal{M}_1 = 0.89 \pm 0.05 \mathcal{M}_\odot$ and $\mathcal{M}_2 = 0.88 \pm 0.04 \mathcal{M}_\odot$ respectively. Both solutions agree with each other within the error ranges. The calculated dynamical parallax of HD 130669 using Al-Wardat’s masses and the orbital parameters of this work is $0.02180'' \pm 0.0025''$, i.e the system is at a distance of $45.85 pc$. On the other hand, the orbital parallax puts the system at a distance of $46.296 pc$. This assures the coincidence between the two solutions.

HD 191854, ADS 13461, HIP 99376: In this paragraph, we follow the same procedure as previously in order to determine the masses and parallax of this system. The procedure gives us a semi-major axis $a = 25.2768 \pm 1.7911$ au, while from the visual solution we obtain $a = 0.449 \pm 0.0001$ arcseconds. Based on that, we deduce the orbital parallax of the system $\pi_{\text{orb}} = 0.0178'' \pm 0.0013''$, which agrees with the Gaia DR3 parallax of $0.01929'' \pm 0.00128''$ (C. Fontanive and D. Bardalez Gagliuffi 2021). Using this new parallax, the total mass of the system is $\mathcal{M}_{\text{total}} = 2.224 \pm 0.0309 \mathcal{M}_\odot$. From the spectroscopic solution, the mass ratio and the individual masses of the system are $q = 1.268 \pm 0.014$, $\mathcal{M}_1 = 1.2438 \pm 0.1377 \mathcal{M}_\odot$ and $\mathcal{M}_2 = 0.9802 \pm 0.0276 \mathcal{M}_\odot$ respectively. At the same time, we obtain from Al-Wardat’s method $q = 1.25 \pm 0.022$, $\mathcal{M}_1 = 1.12 \pm 0.06 \mathcal{M}_\odot$ and $\mathcal{M}_2 = 0.89 \pm 0.04 \mathcal{M}_\odot$. Both solutions agree with each other within the error ranges.

Table 6
The Physical Parameters

Parameters	HD 130669	HD 184467	HD 191854	HD 214222	References
π_{orb} [mas]	21.6 ± 0.3	56.10 ± 0.71	17.80 ± 1.30	14.10 ± 0.23	This work
π_{HIP1} [mas]	24.21 ± 1.29	59.84 ± 0.64	19.45 ± 0.80	13.76 ± 0.79	(M. Perryman et al. 1997)
π_{HIP2} [mas]	22.59 ± 1.23	58.96 ± 0.65	19.48 ± 0.54	14.15 ± 0.74	(F. van Leeuwen 2007)
π_{Gaia1} [mas]	...	58.37 ± 0.54	(A. G. Brown et al. 2016)
π_{Gaia2} [mas]	...	54.87 ± 0.24	19.2965 ± 0.1282	14.235 ± 0.319	(Gaia Collaboration 2018a)
π_{Gaia3} [mas]	...	55.28 ± 0.35	(C. Fontanive & D. Bardalez Gagliuffi 2021)
a^*	0.123 ± 0.001	0.081 ± 0.001	0.449 ± 0.0001	0.1446 ± 0.0001	This work
a_{AU}	5.7042 ± 0.0830	1.444 ± 0.0042	25.2768 ± 1.7911	10.2810 ± 0.1668	This work
e	0.38926 ± 0.00030	0.38926 ± 0.003	0.4922 ± 0.0033	0.36168 ± 0.013	This work
$\mathcal{M}_A (\mathcal{M}_\odot)$	0.9266 ± 0.0511	0.8329 ± 0.0188	1.2438 ± 0.1377	1.1165 ± 0.1958	This work
$\mathcal{M}_B (\mathcal{M}_\odot)$	0.9220 ± 0.0448	0.8122 ± 0.0107	0.9802 ± 0.0276	1.0662 ± 0.1098	This work
$\mathcal{M}_t (\mathcal{M}_\odot)$	1.8486 ± 0.0815	1.6451 ± 0.0217	2.224 ± 0.3091	2.1767 ± 0.2245	This work
T_A	5290	5340	5930	6075	This work
T_B	5230	5185	5440	6000	This work
L_A	0.64	0.51	2.79	1.59	This work
L_B	0.61	0.39	0.65	1.40	This work
Sp_A	F9V	G4V	F7V	G1V	This work
Sp_B	G1V	G8V	G7	G4V	This work

HD 214222, ADS 16098, HIP 111528: Following the same steps as for the other systems, the binary semimajor axis is 10.2810 ± 0.1668 au, while from the visual solution we get $a = 0.1446 \pm 0.0001$ arcseconds. Hence, we calculate the orbital parallax of the system which is found to be $\pi_{orb} = 0.01410'' \pm 0.0023''$ and is in agreement with the Gaia DR2 parallax of $0.01435'' \pm 0.00319''$ (A. G. Brown et al. 2016). Using this parallax value, the combined mass of the system is $\mathcal{M}_t = 1.1165 \pm 0.1958 \mathcal{M}_\odot$. Finally, using the spectroscopic solution, the mass ratio and the individual masses of the system are $q = 1.044 \pm 0.022$, $\mathcal{M}_1 = 1.1165 \pm 0.1958 \mathcal{M}_\odot$ and $\mathcal{M}_2 = 1.0662 \pm 0.1098 \mathcal{M}_\odot$. The Al-Wardat's method for this systems gives $q = 1.01 \pm 0.016$, $\mathcal{M}_1 = 1.12 \pm 0.06 \mathcal{M}_\odot$ and $\mathcal{M}_2 = 1.09 \pm 0.05 \mathcal{M}_\odot$. Both solutions agree with each other within the error ranges.

5.1 Comparison of Mass Ratios

Most systems show strong consistency in mass ratios when comparing calculated and observed values. The results confirm the reliability of the methods used to calculate the masses of binary stars. The mass ratios (q_{calc}) obtained from the combination of astrometric and spectroscopic orbital elements closely match those obtained from solely spectroscopic measurements of radial velocity. For HD 130669, the values are nearly identical ($q_{calc} = 1.005 \pm 0.034$; $q_{spec} = 1.007 \pm 0.016$), as is the case of HD 184467 ($q_{calc} = 1.026 \pm 0.022$; $q_{spec} = 1.0255 \pm 0.0011$) and HD 214222 ($q_{calc} = 1.047 \pm 0.049$; $q_{spec} = 1.0531 \pm 0.016$); see Table 7 (and Table 6), with all differences well within the respective uncertainties. Consequently, the physical parameters derived appear to be highly credible. The discrepancy between the calculated and spectroscopic mass ratio ($q_{calc} = 1.268 \pm 0.058$; $q_{spec} = 1.288 \pm 0.320$) for HD 191854 is the largest among the four systems analyzed. Despite the statistical consistency within uncertainties 1σ , the relatively large error in the spectroscopic ratio suggests potential challenges for the radial velocity solution. There are several explanations for this, including blended spectral lines, moderate orbital inclination reducing velocity amplitudes, and a lack of resolution in the data. Thus, apparent discrepancies are more a reflection of observational uncertainty than methodological inconsistencies. It is recommended to acquire higher resolution spectra and extend temporal coverage to improve the precision of the system's spectroscopic parameters.

Table 7
Comparison of Calculated and Spectroscopic Mass Ratios with Errors

System	$q_{\text{calc}} \pm \sigma_{\text{calc}}$ (This Work)	$q_{\text{spec}} \pm \sigma_{\text{spec}}$ (Spec Orbits)
HD 130669	1.005 ± 0.034	1.007 ± 0.016
HD 184467	1.026 ± 0.022	1.0255 ± 0.0011
HD 191854	1.268 ± 0.058	1.288 ± 0.320
HD 214222	1.047 ± 0.049	1.0531 ± 0.016

6 Dynamical Stability and Habitability

Since we have determined the masses and orbital parameters of our binary systems in the previous sections, here we investigate whether these systems may provide a suitable dynamical environment for hosting planets and whether any of these planets can reside in the habitable zones of the respective systems.

6.1 Dynamical Stability

Although some of the systems may favor the existence of circumbinary planets (the planet being on an orbit around both stars) while some other may favor circumstellar orbits (the planet orbiting one of the stars), we are going to explore both configurations for each system. For the purpose of searching for stable circumbinary orbits, we make use of the work of N. Georgakarakos et al. (2024), while for circumstellar orbits we use the respective formula provided by M. J. Holman and P. A. Wiegert (1999).

For circumbinary planetary orbits, we evaluate the formula for the upper critical semimajor axis (the semimajor axis beyond which all planetary orbits are stable) from N. Georgakarakos et al. (2024). For orbits of planetary eccentricities 0.8 or less, the formula is given by

$$a_o^{cr} = a \cdot 10^k, \quad (8)$$

where a is the binary semi-major axis. For coplanar orbits, the exponent k is given by

$$k = 0.23612 - 0.29377 \log_{10}(M_b) + 1.06753e + 0.62109e_p - 0.21512[\log_{10}(M_b)]^2 - 1.52936e^2 - 0.47480e_p^2 - 0.03932[\log_{10}(M_b)]^3 + 0.87506e^3 + 1.25895e_p^3, \quad (9)$$

with $M_b = \mathcal{M}_B/(\mathcal{M}_A + \mathcal{M}_B)$ and e and e_p are the eccentricities of the binary and the planet, respectively. For initially circular planetary orbits, i.e. $e_p = 0$, the upper critical semi-major axes can be found in Table 8.

In the event that the planetary orbit is assumed to be initially eccentric, then the stability border will be farther away from the stellar binary. This can be seen in Figure 6.

In order to determine the stability status of circumstellar orbits in our binary systems, we make use of the following empirical formula (M. J. Holman and P. A. Wiegert 1999), which is valid for coplanar and initially circular planetary orbits:

$$a_c = (0.464 - 0.380M_b - 0.631e + 0.586M_b e + 0.15e^2 - 0.198M_b e^2)a. \quad (10)$$

The results can be found in Table 9. It is noted that the stability borders around the individual stars of each system are quite similar. This is due to the fact that all our systems consist of stars with similar masses.

Table 8
Stability Borders for Circumbinary Orbits

System	a_o^{cr} (au)
HD 130669	20.94
HD 184467	5.04
HD 191854	96.72
HD 214222	35.23

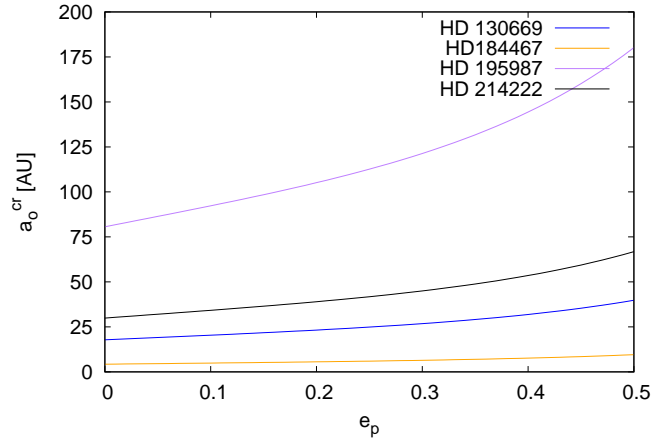


Figure 6: Circumbinary stability curves for the four binary systems HD 130669, HD 184467, HD 191854, and HD 214222. The curves show the critical semi-major axis a_{cr} of a stable circumbinary planet as a function of planet eccentricity e_p , calculated based on the orbital and stellar parameters of each system.

Table 9
Stability Borders for Circumstellar Orbits

Star	a_c (au)
HD 130669A	0.69
HD 130669B	0.69
HD 184467A	0.22
HD 184467B	0.21
HD 191854A	3.30
HD 191854B	2.88
HD 214222A	1.65
HD 214222B	1.61

6.2 Habitability

The discovery of Earth-sized exoplanets has ignited a discussion about the potential of finding life outside our solar system. Determining whether a planet may be habitable is a complex and multifaceted matter (e.g., M. J. Way and N. Georgakarakos 2017; V. S. Meadows and R. K. Barnes 2018; R. Schwarz et al. 2018; M. J. Way et al. 2023). We saw in the previous section that it is possible for planetary bodies to be on stable orbits around the four binary systems of this work. Orbital stability is usually one of the first requirements when looking for potentially habitable planets. A planet needs to be on an orbit that provides a suitable environment for the development of life. Strong gravitational interactions between the stellar binary and a planet can lead to chaotic orbital evolution, which eventually may lead to the ejection of the planet from the system. Therefore, the investigation of the long-term dynamical stability of the planetary orbit is a fundamental requirement when looking for habitable worlds.

We are now going to explore the potential for each one of our systems to host a planet within the respective habitable zone. The habitable zone is the area around a star where a planet with an Earth-like atmosphere and on a circular orbit can retain liquid water on its surface (J. F. Kasting et al. 1993). Planetary systems, however, often consist of more than two bodies (multistar systems or single-star multiplanet systems). This implies that even if the planet is on an initially circular orbit, the latter will evolve into an elliptical one, meaning that the distance between the stars and the planets will vary on different timescales (e.g., N. Georgakarakos 2003; N. Georgakarakos and S. Eggl 2015). This means the classical (or static) habitable zone, as defined previously, may not be an accurate marker for making an initial assessment of the potential habitability status of a planet. In a series of papers, we have developed an analytical method to calculate planetary habitable zones in binary systems or systems with more than one planet, taking into consideration the orbital evolution of our potentially habitable world (S. Eggl et al. 2012; N. Georgakarakos et al. 2018, 2021). A nice review on that matter can be found in S. Eggl et al. (2020).

In the context of that work we defined three types of so-called dynamically informed habitable zones (DIHZ): the permanently habitable zone (PHZ), which is the area around the star(s) where the planet always stays within habitable radiation limits; the averaged habitable zone (AHZ), where the planet is on average within habitable radiation limits; and finally the extended habitable zone (EHZ), where the planet is on average within habitable radiation limits plus or minus one standard deviation. We apply our method to all four binary systems. For circumbinary habitable zones we used the method presented by N. Georgakarakos et al. (2021), while for exploring habitable zones around one of the stars of the binary system, we used results from S. Eggl et al. (2012). A graphical representation of the results can be found in Figure 7. In the calculations that led to these plots, we have allowed the binary eccentricity to vary to observe the effect of that parameter on the DIHZs.

Our calculations revealed that none of our systems have circumbinary habitable zones. This is because the area close to the stars is dynamically unstable; therefore, we cannot determine any habitable zone. The same happens with HD 184467 when looking for circumstellar habitable zones. As we saw from our stability analysis, a planet would need to be very close to either star to survive the gravitational pull of the other one, and therefore, as in the circumbinary scenario, the habitable zones of this system lie in dynamically unstable areas.

On the other hand, as seen in Figure 7, HD 130669, HD 191854, and HD 214222 allow the existence of habitable zones around their stars. Although HD 130669 shows good potential for having habitable zones around its stars, dynamical instability starts to settle into the habitable zone as the binary eccentricity increases. As a result, when the eccentricity reaches the current value of the system, the whole range of the habitable zone is dynamically unstable. The situation is more promising for HD 191854, where even for high values of the binary eccentricity, the PHZ

covers almost the whole extent of the habitable zone. This happens because the system is the widest binary among all four systems under consideration. Finally, HD 214222 stands between the other two systems in terms of the existence of habitable zones around its stellar components, as seen in the bottom row of Figure 7.

7 Concluding Remarks

The present work showcases the effectiveness of integrating precise spectroscopic orbits with high-quality visual observations to obtain an all-inclusive set of orbital and physical parameters for four double-lined spectroscopic binaries: HD 130669, HD 184467, HD 191854, and HD 214222. By refining the orbital parallax, individual masses, and orbital separations, this approach resolves earlier discrepancies found in Hipparcos and Gaia (DR1/DR2/EDR3) measurements and results in more accurate distance and mass estimates.

By applying Al-Wardat’s spectrophotometric modeling technique, it was possible to estimate the essential stellar properties of each component, such as temperatures, luminosities, and radii. This information then facilitated an evaluation of whether these systems could support stable, habitable environments for any potential orbiting planets. Figure 8 presents all the previous steps and summarizes what we have accomplished in this work. In particular,

1. Accurate masses and orbital parallaxes. Combining the spectroscopic mass ratio with top-tier visual orbits produced well-defined values for the total and individual stellar masses. This integrated method also allowed for an independent calculation of the orbital parallax, which generally aligns well with and refines both Hipparcos and Gaia data.
2. Consistency of mass ratios. The calculated and spectroscopic mass ratios agreed closely for HD 130669 and HD 184467, and were similarly consistent for HD 214222. On the other hand, HD 191854 displayed larger uncertainties, suggesting that further observations may be needed to reduce measurement errors.
3. Stable orbital configurations. Preliminary stability analyses indicate that some of these binary systems could support circumstellar or circumbinary planets, depending on orbital size and eccentricity. While stable orbits are feasible for specific configurations, higher eccentricities can limit or undermine the habitable zone.
4. Habitability potential. For systems with intermediate eccentricities and sufficiently separated stellar components, there may be regions where terrestrial planets could maintain liquid water at the surface. Even so, the specific range of habitability will hinge on both orbital geometry and stellar properties.

Overall, this study underscores the importance of integrating multiple observation techniques — spectroscopic, astrometric, and interferometric — to attain accurate orbits and stellar properties in multiple-star systems. Such high-precision data are essential for understanding planet formation and the likelihood of habitable conditions around Sun-like stars in binary environments.

Figure 8 summarizes the methodological workflow applied in this study, from data acquisition and orbital modeling to the final habitability and dynamical stability assessments. By combining spectroscopic and visual analysis of SB2 systems, we can determine precise physical and orbital parameters that are necessary for assessing dynamical stability and habitability. Spectroscopic and calculated mass ratios are in good agreement, validating the robustness of the methods used and demonstrating the importance of multitechnique approaches. It will also be possible to apply this methodology to larger samples of SB2 systems once Gaia DR4 is released, which will increase astrometric precision and orbital accuracy. Incorporating more targets and extending observational baselines will increase the statistical power of habitability assessments. Further interferometric

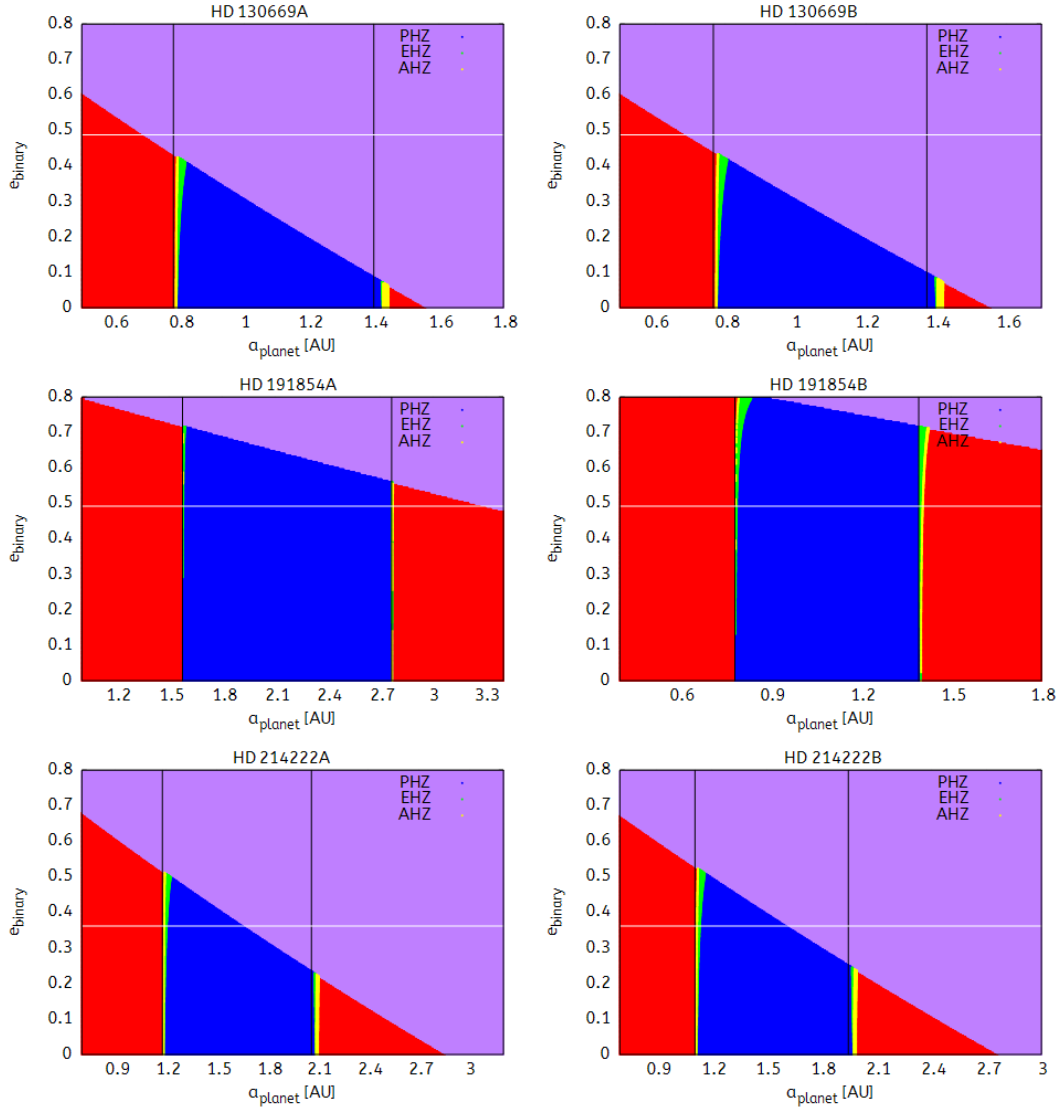


Figure 7: Circumstellar habitable zones for HD 130669, HD191854, and HD214222. Blue color: PHZ, yellow color: AHZ, green color: EHZ, red color: uninhabitable area, purple color: areas of dynamical instability. The white line marks the eccentricity of the stellar binary, while the vertical black lines are the borders of the classical habitable zone.

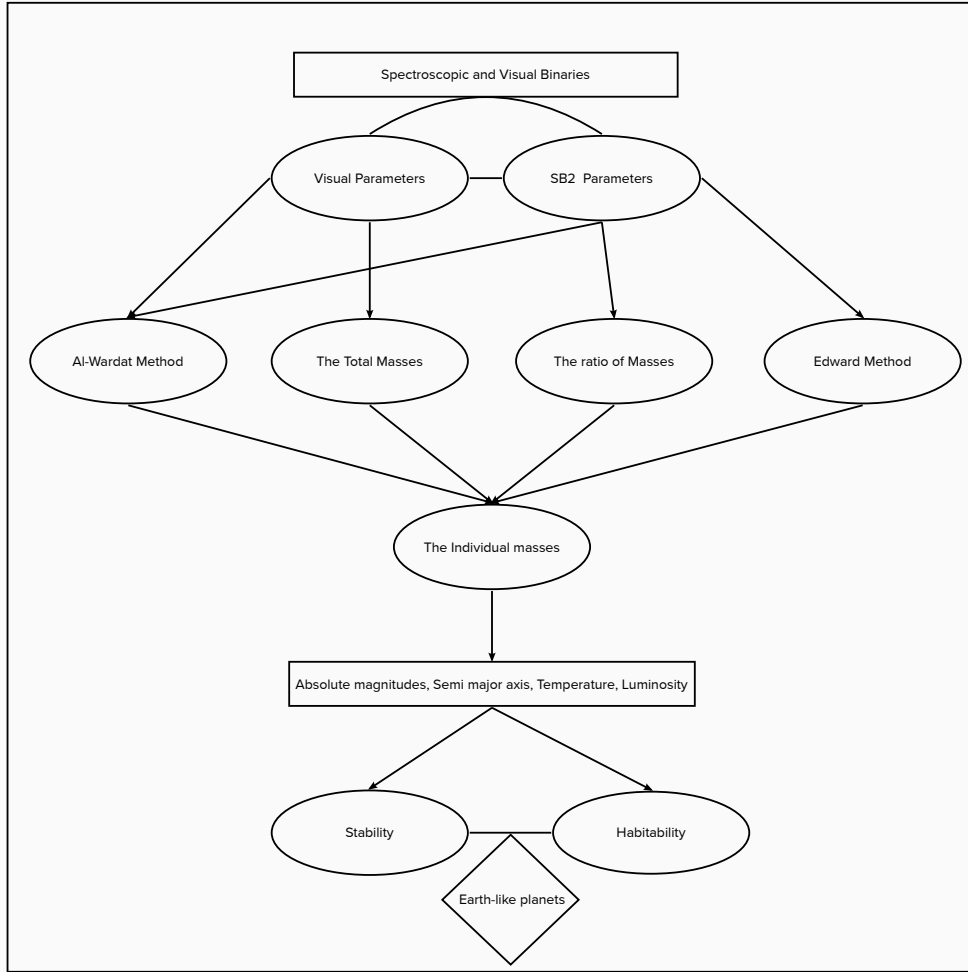


Figure 8: A flowchart of the methodology used in this work.

observations and high-resolution spectroscopic observations will help refine orbital inclinations and resolve small-angle distance systems. It will be possible to gain a deeper understanding of planet-hosting potential in binary environments as a result of these developments.

Acknowledgments

We are grateful to the US Naval Observatory for both the Fourth Catalog of Interferometric Observations of Binary Stars and the Washington Double Star Catalog. Also to Centre de données astronomiques de Strasbourg (CDS), Strasbourg, France, for the available SIMBAD database. This work has made use of data from the European Space Agency (ESA) mission Gaia (<https://www.cosmos.esa.int/gaia>), processed by the Gaia Data Processing and Analysis Consortium (DPAC; <https://www.cosmos.esa.int/web/gaia/dpac/consortium>). It also has made use of SAO/NASA, the SIMBAD database, the Fourth Catalog of Interferometric Measurements of Binary Stars, IPAC

data systems, and codes of Al-Wardat's method for analyzing binary and multiple stellar systems.

ORCID iDs

Ahmad Abushattalaa <https://orcid.org/0000-0002-7796-6562>
Nikolaos Georgakarakosaa <https://orcid.org/0000-0002-7071-5437>
Mashhoor A. Al-Wardataa <https://orcid.org/0000-0002-1422-211X>
Hassan B. Haboubiaa <https://orcid.org/0009-0004-7254-0724>
Deshinta Arrova Dewiaa <https://orcid.org/0000-0003-1488-7696>
Enas M. Abu-Alrobaa <https://orcid.org/0000-0001-7718-9209>
Abdallah M. Husseinaa <https://orcid.org/0000-0002-0738-4305>

References

- Abushattal, A., Al-Wardat, M., Taani, A., Khassawneh, A., and Al-Naimiy, H. 2019, *JPCS*, 1258, 012018
- Abushattal, A., Alrawashdeh, A., and Kraishan, A. 2022a, *CoBAO*, 69, 251
- Abushattal, A., Kraishan, A., and Alshamaseen, O. 2022b, *CoBAO*, 69, 235
- Abushattal, A. A., Al-Wardat, M. A., Horch, E. P., et al. 2024, *AdSpR*, 73, 1170
- Abushattal, A. A., Docobo, J. A., and Campo, P. P. 2019b, *AJ*, 159, 28
- Abushattal, A. A. M. 2017, PhD thesis, Universidade de Santiago de Compostela
- Al-Tawalbeh, Y. M., Hussein, A. M., Taani, A. A., et al. 2021, *AstBu*, 76, 71
- Al-Wardat, M. 2002a, *BSAO*, 53, 58
- Al-Wardat, M. 2002b, *ESASP*, 53, 51
- Al-Wardat, M. 2007, *AN*, 328, 63
- Al-Wardat, M. 2008, *AstBu*, 63, 361
- Al-Wardat, M. 2009, *AN*, 330, 385
- Al-Wardat, M. 2012, *PASA*, 29, 523
- Al-Wardat, M., Balega, Y. Y., Leushin, V., et al. 2014a, *AstBu*, 69, 58
- Al-Wardat, M., Balega, Y. Y., Leushin, V., et al. 2014b, *AstBu*, 69, 198
- Al-Wardat, M., Docobo, J., Abushattal, A., and Campo, P. 2017a, *AstBu*, 72, 24
- Al-Wardat, M., Docobo, J., Abushattal, A., and Campo, P. 2017b, *AstBu*, 72, 24
- Al-Wardat, M., and Widyan, H. 2009, *AstBu*, 64, 365
- Al-Wardat, M. A. 2002, *BSAO*, 53, 51
- Al-Wardat, M. A. 2007, *AN*, 328, 63
- Al-Wardat, M. A. 2009, *AN*, 330, 385
- Al-Wardat, M. A. 2012, *PASA*, 29, 523
- Al-Wardat, M. A., El-Mahameed, M. H., Yusuf, N. A., Khasawneh, A. M., and Masda, S. G. 2016, *RAA*, 16, 166
- Al-Wardat, M. A., Hussein, A. M., Al-Naimiy, H. M., and Barstow, M. A. 2021a, *PASA*, 38, e002
- Al-Wardat, M. A., Abu-Alrob, E., Hussein, A. M., et al. 2021b, *RAA*, 21, 161
- Alameryeen, H., Abushattal, A., and Kraishan, A. 2022, *CoBAO*, 69, 242
- Alnaimat, B., Abushattal, A., Kraishan, A., and Alnaimat, M. 2022, *CoBAO*, 69, 223
- Alnaimat, S., Jameel, R., Abushattal, A., and Al-Wardat, M. 2025, in *Proc. 14th Arabic Conf. Arab Union for Astronomy and Space Sciences: AUASS-CONF23*, Vol. 420 (Berlin: Springer Nature)
- Armstrong, J. T., Clark III, J. H., Gilbreath, G. C., et al. 2004, *Proc. SPIE*, 5491, 1700

Balega, I., Bonneau, D., and Foy, R. 1984, *A&AS*, 57, 31
 Bonneau, D., Balega, Y., Blazit, A., et al. 1986, *A&AS*, 65, 27
 Borucki, W. J. 2016, *RPPh*, 79, 036901
 Brown, A. G., Vallenari, A., Prusti, T., et al. 2016, *A&A*, 595, A2
 Christy, J. W., and Walker, R. 1969, *PASP*, 643
 Docobo, J., Balega, Y., Campo, P., and Abushattal, A. 2018, *WDS*, 196, 1
 Docobo, J., Balega, Y., Ling, J., Tamazian, V., and Vasyuk, V. 2000, *AJ*, 119, 2422
 Docobo, J., Campo, P., Gomez, J., and Horch, E. P. 2018c, *AJ*, 156, 185
 Docobo, J., Elipe, A., and Abad, A. 1988, *Ap&SS*, 142, 195
 Docobo, J. A. 1985, *CeMec*, 36, 143
 Docobo, J. A. 2012, in *Orbital Couples: Pas de Deux in the Solar System and the Milky Way*, ed. F. Arenou and D. Hestroffer (Paris: Observatoire de Paris), 119
 Docobo, J. A., Campo, P. P., Andrade, M., and Horch, E. P. 2014, *AstBu*, 69, 461
 Docobo, J. A., Griffin, R. F., Campo, P. P., and Abushattal, A. A. 2017, *MNRAS*, 469, 1096
 Drimmel, R., Bucciarelli, B., and Inno, L. 2019, *RNAAS*, 3, 79
 Duchêne, G., and Kraus, A. 2013, *ARA&A*, 51, 269
 Duquenois, A., and Mayor, M. 1991, *A&A*, 248, 485
 Edwards, T. 1976, *AJ*, 81, 245
 Eggen, O. 1965, *AJ*, 70, 19
 Eggen, O. J. 1955, *PASP*, 67, 169
 Eggl, S., Georgakarakos, N., and Pilat-Lohinger, E. 2020, *Galax*, 8, 65
 Eggl, S., Pilat-Lohinger, E., Georgakarakos, N., Gyergovits, M., and Funk, B. 2012, *ApJ*, 752, 74
 Esa 1997, *yCat*, I/239, 323, L49–L52
 Fardal, M. A., van der Marel, R., del Pino, A., and Sohn, S. T. 2021, *AJ*, 161, 58
 Farrington, C. D., Ten Brummelaar, T., Mason, B., et al. 2010, *AJ*, 139, 2308
 Fontanive, C., and Bardalez Gagliuffi, D. 2021, *FrASS*, 8, 16
 Gaia Collaboration, Brown, A. G. A., Vallenari, A., et al. 2021, *A&A*, 649, A1
 Gaia Collaboration, et al. 2018a, *yCat*, 1345, 0
 Gaia Collaboration, Mignard, F., Klioner, S., et al. 2018b, *A&A*, 616, A14
 Gaspar, A., Rieke, G. H., and Ballering, N. 2016, *ApJ*, 826, 171
 Georgakarakos, N. 2003, *MNRAS*, 345, 340
 Georgakarakos, N., and Eggl, S. 2015, *ApJ*, 802, 94
 Georgakarakos, N., and Eggl, S. 2019, *MNRAS*, 487, L58
 Georgakarakos, N., Eggl, S., Ali-Dib, M., and Dobbs-Dixon, I. 2024, *AJ*, 168, 224
 Georgakarakos, N., Eggl, S., and Dobbs-Dixon, I. 2018, *ApJ*, 856, 155
 Georgakarakos, N., Eggl, S., and Dobbs-Dixon, I. 2021, *FrASS*, 8, 44
 Girardi, L., Bressan, A., Bertelli, G., and Chiosi, C. 2000, *A&AS*, 141, 371
 Griffin, R. F. 2012, *Obs*, 132, 309
 Griffin, R. F. 2015, *Obs*, 135, 321
 Heintz, W. 1997, *ApJS*, 111, 335
 Hog, E., Fabricius, C., Makarov, V. V., et al. 2000, Technical Report, Naval Observatory, Washington, DC
 Holman, M. J., and Wiegert, P. A. 1999, *AJ*, 117, 621
 Horch, E. P., Veillette, D. R., Gallé, R. B., et al. 2009, *AJ*, 137, 5057
 Horch, E. P., Van Altena, W. F., Demarque, P., et al. 2015, *AJ*, 149, 151
 Howell, S. B., Scott, N. J., Matson, R. A., et al. 2021, *FrASS*, 8, 10
 Hussein, A. M., Al-Wardat, M. A., Abushattal, A., et al. 2022, *AJ*, 163, 182
 Jack, D., Hernández Huerta, M. A., and Schröder, K.-P. 2020, *AN*, 341, 616

Kasting, J. F., Whitmire, D. P., and Reynolds, R. T. 1993, *Icar*, 101, 108
 Keenan, P. C., and McNeil, R. C. 1989, *ApJS*, 71, 245
 Kiefer, F., Halbwegs, J.-L., Lebreton, Y., et al. 2018, *MNRAS*, 474, 731
 Labeyrie, A. 1970, *A&A*, 6, 85
 Lester, K. V., Gies, D. R., Schaefer, G. H., et al. 2019a, *AJ*, 157, 140
 Lester, K. V., Gies, D. R., Schaefer, G. H., et al. 2019b, *AJ*, 158, 218
 Lester, K. V., Fekel, F. C., Muterspaugh, M., et al. 2020, *AJ*, 160, 58
 Masda, S., Docobo, J., Hussein, A., et al. 2019a, *AstBu*, 74, 464
 Masda, S. G., Al-Wardat, M. A., Neuhäuser, R., and Al-Naimiy, H. M. 2016, *RAA*, 16, 112
 Masda, S. G., Al-Wardat, M. A., and Pathan, J. K. M. K. 2018, *RAA*, 18, 072
 Masda, S. G., Al-Wardat, M. A., and Pathan, J. M. 2019b, *RAA*, 19, 105
 Matson, R. A., Howell, S. B., Horch, E. P., and Everett, M. E. 2018, *AJ*, 156, 31
 McAlister, H., Hendry, E., Hartkopf, W., Campbell, B., and Fekel, F. 1983, *ApJS*, 51, 309
 McAlister, H. A. 1976, *PASP*, 88, 957
 McAlister, H. A. 1977, *ApJ*, 212, 459
 McAlister, H. A. 1978, *ApJ*, 223, 526
 Meadows, V. S., and Barnes, R. K. 2018, in *Handbook of Exoplanets*, ed. H. J. Deeg and J. A. Belmonte, Vol. 57 (Berlin: Springer)
 Michel, K.-U., and Mugrauer, M. 2021, *FrASS*, 8, 14
 Mitrofanova, A., Dyachenko, V., Beskakatov, A., et al. 2021, *AJ*, 162, 156
 Netopil, M. 2017, *MNRAS*, 469, 3042
 Perryman, M., et al. 1997, *star*, 2, 2
 Piccotti, L., Docobo, J. Á., Carini, R., et al. 2020, *MNRAS*, 492, 2709
 Pilat-Lohinger, E., and Bazsó, Á. 2021, *FrASS*, 8, 47
 Pourbaix, D. 2000, *A&AS*, 145, 215
 Pourbaix, D., Tokovinin, A. A., Batten, A. H., et al. 2004, *A&A*, 424, 727
 Prusti, T., De Bruijne, J., Brown, A. G., et al. 2016, *A&A*, 595, A1
 Raghavan, D., McAlister, H. A., Henry, T. J., et al. 2010, *ApJS*, 190, 1
 Ren, S., and Fu, Y. 2010, *AJ*, 139, 1975
 Ricker, G. R., Latham, D., Vanderspek, R., et al. 2010, *AAS*, 215, 450
 Roman, N. G. 1955, *ApJS*, 2, 195
 Schwarz, R., Bazsó, Á., Georgakarakos, N., et al. 2018, *MNRAS*, 480, 3595
 Soubiran, C., Le Campion, J.-F., Brouillet, N., and Chemin, L. 2016, *A&A*, 591, A118
 Starikova, G. 1978, *SvAL*, 4, 296
 Stassun, K. G., and Torres, G. 2018, *ApJ*, 862, 61
 Taani, A., Abushattal, A., and Mardini, M. K. 2019, *AN*, 340, 847
 Tokovinin, A. 1992a, *International Astronomical Union Colloquium*, Vol. 135 (Cambridge: Cambridge Univ. Press), 573
 Tokovinin, A. 1992b, *A&A*, 256, 121
 Tokovinin, A. 2014, *AJ*, 147, 86
 Tokovinin, A., and Horch, E. P. 2016, *AJ*, 152, 116
 Tokovinin, A., Mason, B. D., Mendez, R. A., Horch, E. P., and Briceño, C. 2019, *AJ*, 158, 48
 van Leeuwen, F. 2007, *A&A*, 474, 653
 Vasiliev, E. 2019, *MNRAS*, 489, 623
 Wang, X.-L., Ren, S.-L., and Fu, Y.-N. 2016, *RAA*, 16, 033
 Way, M. J., and Georgakarakos, N. 2017, *ApJL*, 835, L1
 Way, M. J., Georgakarakos, N., and Clune, T. L. 2023, *AJ*, 166, 227
 Wenger, M., Ochsenein, F., Egret, D., et al. 2000, *A&AS*, 143, 9

Yousef, Z. T., Annuar, A., Hussein, A. M., et al. 2021, RAA, 21, 114
Zinn, J. C., Huber, D., Pinsonneault, M. H., and Stello, D. 2017, ApJ, 844, 166